Selective growth of single phase VO2(A, B, and M) polymorph thin films

Amar Srivastava, Helene Rotella, Surajit Saha, Banabir Pal, Gopinadhan Kalon, Sinu Mathew, Mallikarjuna Motapothula, Michal Dykas, Ping Yang, Eiji Okunishi, D. D. Sarma, and T. Venkatesan

Citation: APL Mater. **3**, 026101 (2015); doi: 10.1063/1.4906880
View online: http://dx.doi.org/10.1063/1.4906880
View Table of Contents: http://scitation.aip.org/content/aip/journal/aplmater/3/2?ver=pdfcov
Published by the AIP Publishing

Selective growth of single phase VO_2(A, B, and M) polymorph thin films

Amar Srivastava,[1,2] Helene Rotella,[2,3] Surajit Saha,[1,2] Banabir Pal,[4] Gopinadhan Kalon,[2] Sinu Mathew,[2] Mallikarjuna Motapothula,[2] Michal Dykas,[2] Ping Yang,[3] Eiji Okunishi,[5] D. D. Sarma,[4,6] and T. Venkatesan[1,2,3,a]

[1]*Department of Physics, National University of Singapore, Singapore 117542*
[2]*NUSNNI-NanoCore, National University of Singapore, Singapore 117576*
[3]*Singapore Synchrotron Light Source, National University of Singapore, 5 Research Link, Singapore 117603*
[4]*Solid State and Structural Chemistry Unit, Indian Institute of Science, Bangalore 560012, India*
[5]*Electron Optics Division, JEOL Ltd., Tokyo 196-8558, Japan*
[6]*Council of Scientific and Industrial Research-Network of Institutes for Solar Energy (CSIR-NISE), New Delhi 110001, India*

(Received 10 October 2014; accepted 16 January 2015; published online 3 February 2015)

We demonstrate the growth of high quality single phase films of VO_2(A, B, and M) on $SrTiO_3$ substrate by controlling the vanadium arrival rate (laser frequency) and oxidation of the V atoms. A phase diagram has been developed (oxygen pressure versus laser frequency) for various phases of VO_2 and their electronic properties are investigated. VO_2(A) phase is insulating VO_2(B) phase is semi-metallic, and VO_2(M) phase exhibits a metal-insulator transition, corroborated by photoelectron spectroscopic studies. The ability to control the growth of various polymorphs opens up the possibility for novel (hetero)structures promising new device functionalities. [http://dx.doi.org/10.1063/1.4906880]

Transition metal oxides are used in a wide range of practical applications such as photocatalysts,[1] cathode materials,[2,3] gas sensors,[4] optical switching devices,[5] and intelligent thermo-chromic windows.[6] They also exhibit various polymorphic structures, among which many are neither stable in ambient conditions nor can be easily synthesized. These metastable phases have been the subject of considerable interest due to their unique and superior physical and chemical properties. Among those functional complex oxides, vanadium oxides can adopt a wide range of V:O ratios, resulting in different structural motifs with various types of coordination polyhedra.[7] In this class, vanadium dioxide (VO_2) exhibits a number of polymorphic forms, such as VO_2(M1), VO_2(M2), VO_2(M3), VO_2(R), VO_2(A), VO_2(B), and VO_2(C). The two layered polymorphs VO_2(A) and VO_2(B) are promising materials for science and technology. VO_2(A) is important for the study of strong electronic correlations resulting from structure and VO_2(B) is important for its use as electrode materials for batteries. Various preparation techniques have been used and developed to stabilize these phases in bulk and thin film forms.[8,9] Using Pulsed Laser Deposition (PLD) technique, thin films of these polymorphs (M1, M2, M3, and R) have been stabilized by substrate engineering[10,11] as well as by adding dopant, such as, Cr.[12] In 1989, Oka *et al.*,[13] reported for the first time the stabilization of polycrystalline powder of VO_2(A) using hydrothermal synthesis. They observed a weak metal-semiconductor transition at 162.8 °C. They related this behavior to a crystallographic transition between a low temperature phase (LTP, space group *P4/ncc*, No. 130) and a high temperature phase (HTP, space group

[a]Author to whom correspondence should be addressed. Electronic mail: venky@nus.edu.sg. Telephone: +65-65165187. Fax: +65-68725563.

$I4/m$, No. 87). In the following year, Oka *et al.*[14] reported the VO_2(B) powder stabilization with a monoclinic structure (space group $C2/m$, No. 12) which underwent a structural evolution occurring over a temperature range from 180 to 300 K. There are several recent reports on A and B phases in the form of bulk and nano powders where thermal annealing causes them to revert to stable VO_2(M) phase.[12] Furthermore, Raman and differential thermal analysis measurements on nanorods of VO_2(A) unravel the metastability of the phase.[13] On the other hand, VO_2(B) films showing a single phase by X-ray diffraction were demonstrated[15] but these samples were insulating in contrast to the expected metallic behavior. Despite these studies, a full understanding of electronic and optical properties of VO_2(A) and VO_2(B) thin films is still missing. Finding ways to synthesize specific VO_2 polymorphs with defined properties will open up channels for new device designs.

In this study, we grew epitaxial, single phase tetragonal VO_2(A), and monoclinic VO_2(B) thin films on (100)$SrTiO_3$(STO) substrates using PLD and compare their structural and transport behavior with VO_2(M) phase films. Cross-sectional transmission electron microscopy (TEM) measurements were done using an aberration-corrected STEM (JEM-ARM200F) facility at JEOL Ltd., Japan. The electrical transport measurements were done in the linear four probe geometry using PPMS Quantum design. The hall voltage measurements on the VO_2 polymorphic thin films were done in the standard van der Pauw arrangement in a DC magnetic field up to 2 T. A commercial vanadium single crystal (100) orientated metal target with 5N purity (from Goodfellow) is used for all the vanadium oxide film growth. The laser energy density and temperature of the substrate were fixed at ~2 J cm^{-2} and 500 °C, respectively, during the optimization of film growth parameters. By varying the laser frequency at a constant energy density, we change the arrival rate of atoms to the surface. By tuning the oxygen background pressure, we also change the oxidation of vanadium both in the plume and on the substrate. This enabled us to study the effect of vanadium arrival rate and the background oxygen pressure on the stability of the metastable phases VO_2(A) and VO_2(B) which were never realized in the thin film form before in a single phase with the expected transport properties.

Figs. 1(a) and 1(b) depict the possible epitaxial relation of VO_2(A) and VO_2(B) bulk unit cell on (100)STO substrate, respectively. At room temperature, VO_2(A) bulk adopts a tetragonal unit cell (u.c.) [a_A = 8.44 Å, b_A = 8.44 Å, and c_A = 7.666 Å] with a space group P4/ncc (No. 130). VO_2(A) can sit on the STO unit cell with the following relation: $\sqrt{2}a_{VO_2(A)}$ (= 11.934 Å) ≅ $3a_{STO}$ (= 11.715 Å), $c_{VO_2(A)}$(= 7.666 Å) ≅ $2a_{STO}$(= 7.810 Å). VO_2(B) bulk, on the other hand, has a monoclinic unit cell [a_B = 12.093 Å, b_B = 3.702 Å, and c_B = 6.433 Å, β = 106.97°], with a space group C2/m (No. 12), which can sit on the STO unit cell as follows: $a_{VO_2(B)}$ (= 12.093 Å) ≅ $3a_{STO}$ (= 11.715 Å), $b_{VO_2(B)}$ (= 3.702 Å) ≅ a_{STO}(= 3.905 Å).[15,16] Thus, one expects a coincident lattice site model to apply here. In the later part of the paper dealing with the TEM cross section results indeed, this is seen to be true. The films of VO_2 M, A, and B under investigation are of thicknesses 60 nm, 60 nm, 40 nm, respectively, confirmed by Rutherford back scattering (RBS) and TEM. The 2D XRD patterns are recorded for all samples of the series (see supplementary material for X-Ray reciprocal space map using 2D detector, Fig. S1[17]). The 1D XRD patterns shown in Fig. 1(c) are extracted from 2D XRD patterns by integrating the intensity along the χ direction. We observed that the VO_2(M) phase reflections are not aligned in χ with the substrate, while for VO_2(A) and VO_2(B), reflections are perfectly aligned with the substrate (χ = 0). At low pressure (1×10^{-4} Torr), M phase is stabilized with the off-chi peaks at 2θ = 27.89°, assigned to (011) crystallographic plane of VO_2(M). By increasing the pressure to 7.5×10^{-4} Torr, we produced a mixture of M and A phases where the peak at 2θ = 29.62° is assigned to (220) plane of VO_2(A) phase,[16] while a single phase VO_2(A) film is stabilized at and above a pressure of 5×10^{-3} Torr. Intriguingly, at the same oxygen pressure, reduction of the laser frequency to 2 Hz gave rise to a single phase VO_2(B) film. A peak at 2θ = 29.05° in the XRD pattern is assigned to (002) plane of VO_2(B) phase.[15] The effect of oxygen partial pressure and laser frequency on the stability of these polymorphs were explored and a phase diagram is established (Fig. 1(d)) for different phases of VO_2. The rocking curves were recorded on each sample in order to check the crystallinity (see supplementary material for rocking curve, Fig. S2[17]). VO_2(A) shows a high crystalline quality (FWHM = 0.1°), while the crystal quality decreases for VO_2(B) (FWHM = 0.6°) and VO_2(M) (FWHM = 0.9°) phases (see supplementary material for comparison of the rocking curves and the calculated d spacings, Table S1[17]). We have further verified the stoichiometry of VO_2(A) and VO_2(B)

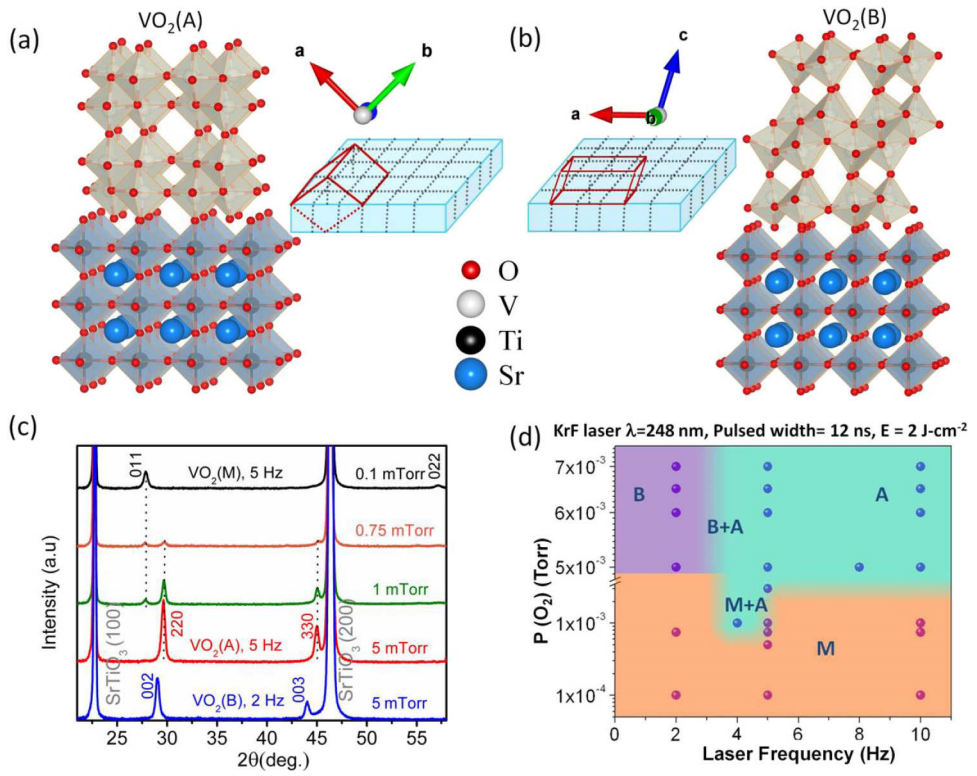

FIG. 1. Schematic crystal structure representation of (a) 220 orientated VO_2(A), (b) 002 orientated VO_2(B) grown on (100) orientated STO substrate. (c) XRD θ-2θ patterns showing different phases for VO_2 thin films. (d) Phase diagram for different polymorphs of VO_2 thin film grown by the PLD.

films using oxygen resonance Rutherford back scattering technique which confirms the composition to be $VO_{2\pm0.02}$ (see supplementary material for oxygen resonance Rutherford backscattering spectra, Fig. S3[17]).

If we look at the various phases of VO_2, they all have different V–V inter-atomic distances.[18] One can empirically understand the type of bond length formed between the V–V due to V–V and V–O–V atomic interactions and its dependence on the influence of the surrounding oxygen. At lower oxygen growth pressures, the atomic interactions are likely to favor shorter V–V distances. At low oxygen pressures, VO_2(R) phase is preferred at the growth temperature which subsequently results in the M phase at room temperature due to the metal-insulator transition (MIT). When the oxygen pressure is increased, the A phase with a longer average V–V distance[19] may be favored. Further, by decreasing the V arrival rate (i.e., lowering the laser frequency), the B phase with the longest V–V distance is stabilized.[14] Moreover, the symmetry of the phases could also be an important factor for their stabilization. The relatively more symmetric structure of VO_2(A) over VO_2(B) suggests VO_2(A) to be more stable over a wide range of laser frequency. Our explanation is rather qualitative. The actual process can be much more complicated which might involve type of connectivity of the anion sublattice, e.g., number of corner, edge, or face sharing oxygen octahedra. Also, the high degree of structural imperfections suggests that defect formation at the interface (as seen in the TEM images in Fig. 2) might play a critical role as well.

Figs. 2(a)–2(e) and Figs. 2(h)–2(l) present the processed atomic resolution high angle annular dark field-scanning transmission electron microscopy (HAADF-STEM) images of VO_2(A) and VO_2(B) thin films, respectively. The brighter spots represent V atoms, while the position of oxygen rows between the V rows is not resolved. For VO_2(A), the V atoms in 001 domains (Figs. 2(a) and 2(b)) are arranged in a square form separated by O planes aligned along [110] and $[\bar{1}10]$ directions as depicted in Fig. 2(f). In the $\bar{1}10$ domain (rotated by 90° with respect to 001 domain), shown in Figs. 2(a) and 2(c) and modeled in Fig. 2(g), V atoms are arranged in pair of chains separated by O planes

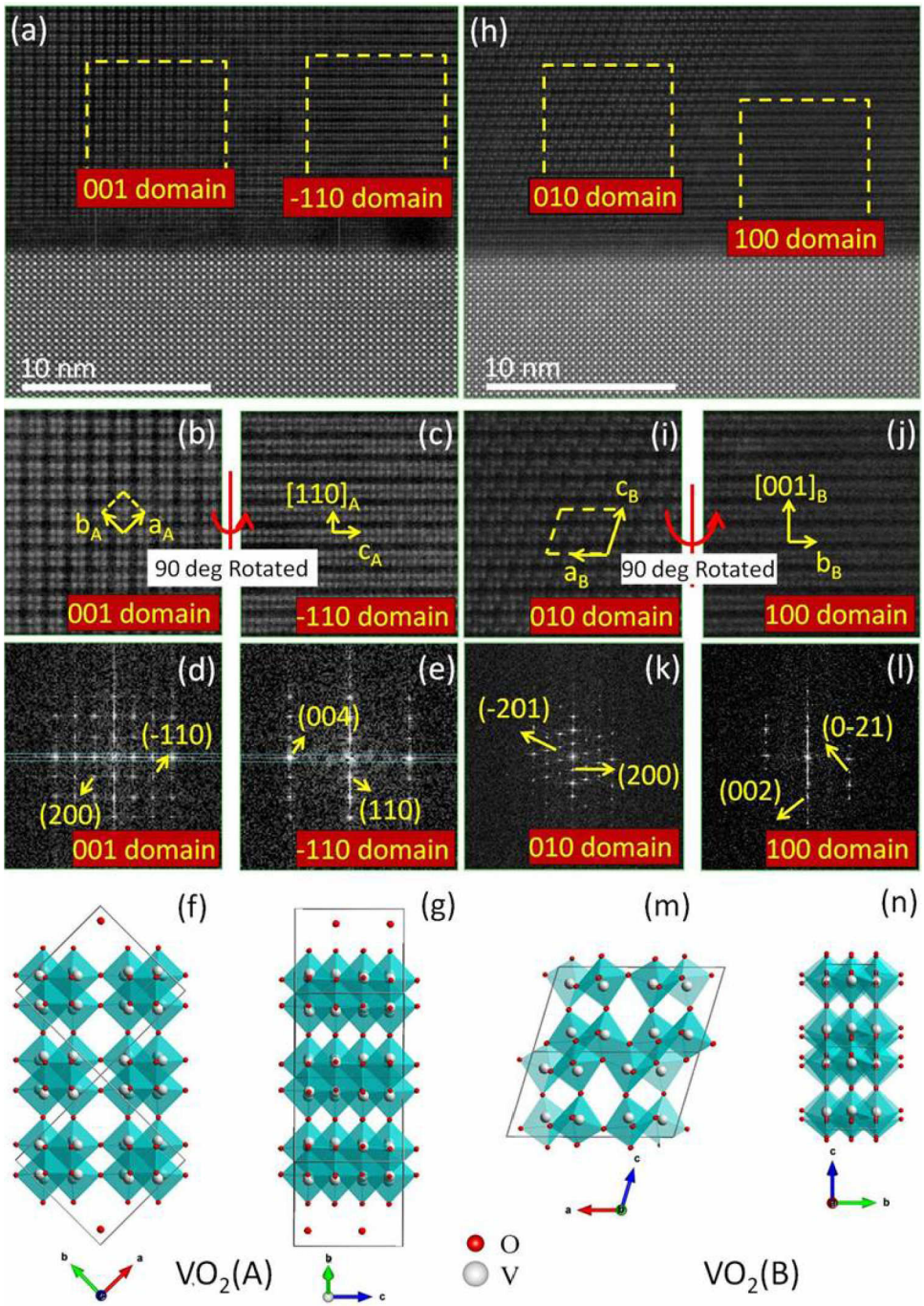

FIG. 2. Processed atomic resolution HAADF-STEM images of cross sectional (a) VO_2(A) and (h) VO_2(B) thin films. (b) and (c) are enlarged 001 and $\bar{1}10$ domains, respectively, in VO_2(A), while (i) and (j) are zoomed 010 and 100 domains, respectively, in VO_2(B). (d), (e), (k), and (l) are the FFT patterns of the four respective domains, while (f), (g), (m), and (n) are sketching the epitaxial relations of VO_2(A) and VO_2(B) with respect to STO substrate.

aligned along [001] direction. Similarly, VO_2(B) contains 010 domains (Fig. 2(i)) where the V atoms are arranged in a parallelogram separated by O planes, consistent with the bulk structure oriented along [010] direction (Fig. 2(m)). Rotated by 90°, 100 domains show a pair of V atom chains separated by O plane, consistent with the bulk structure oriented along [100] direction (Fig. 2(n)). The processed FFT on each domain for the two films VO_2(A) (Figs. 2(d) and 2(e)) and VO_2(B) (Figs. 2(k) and 2(l))

confirms the respective tetragonal and monoclinic symmetry of the films. From these HAADF-STEM image analyses, we can conclude that the VO_2(A) and VO_2(B) thin films present a structure expected from bulk studies.[14,16] The thin film microstructure studies underline the presence of 90°-oriented crystallographic domains in both samples. The epitaxial relationship for VO_2(A) and VO_2(B) can be written as [110]VO_2(A)‖[100]STO and [001]VO_2(A)‖[100]STO or $[\bar{1}10]$ VO_2(A)‖[100]STO and [001]VO_2(B)‖[100]STO and [100]VO_2(B)‖[100]STO or [010]VO_2(B)‖[100]STO, respectively. As part of this TEM analysis, we evaluate the interplanar distances in VO_2(A) and VO_2(B) thin films. For VO_2(A), d_{110} = 6.05(1) Å and d_{001} = 7.75(1) Å are both expanded by ~1.3% compared to the bulk values (d_{110} = 5.968 Å and d_{001} = 7.666(1) Å). However, we observed that VO_2(A) preserves a tetragonal structure in thin film, thus these results suggest that the entire unit cell volume of VO_2(A) has increased. On the other hand, in VO_2(B), the out-of-plane d_{001} = 6.14(1) Å is close to the bulk value (6.153 Å), while the in-plane, d_{100} = 11.85(1) Å and d_{010} = 3.83(1) Å are compressed and elongated, respectively, compared to the bulk values (d_{100} = 12.093(1) Å and d_{010} = 3.7021(2) Å). The evaluated β angle (~107.3(1)°) is very close to the bulk reported value[14] 106.97°. In the TEM, the films do look coherent with respect to the substrate which may be a consequence of the coincident lattice but we noticed in both the A and B phases a ~1 nm buffer layer different from that of the A or B phase which surprisingly preserve the coherence of the over layer with respect to the substrate. Further analysis is under investigation to characterize precisely this buffer layer which is beyond the scope of this paper.

Electrical transport has been measured on the various phases of VO_2 as shown in Fig. 3. The resistivity vs temperature behavior of VO_2(M) is in good agreement with the literature.[20,21] In the high temperature metallic phase, the resistivity is relatively temperature-independent and attains 3×10^{-4} Ω cm at 400 K. In the semiconducting state, the resistivity reaches to 1×10^{-1} Ω cm at 300 K. The transition temperature during the heating cycle is ~340 K which matches with the literature[20] while it shifts to 330 K during cooling cycle with a hysteresis of 10 K (see supplementary material for dlog(R)/dT versus temperature plot, Fig. S4[17]). The VO_2(A) film shows a typical semiconducting behavior with a resistivity of 17 Ω cm at room temperature which drops to 0.3 Ω cm at 550 K. VO_2(B) films exhibit a change of 4 orders (from 4 m Ω cm to 22 Ω cm) in resistivity while cooling from 400 K to 150 K accompanied by a persistent hysteresis during the thermal cycle which is consistent with reports in bulk VO_2(B).[22] These measurements confirm that VO_2(A) is insulating, VO_2(M) is semiconducting, while VO_2(B) is semimetal at room temperature. Figs. 4(a)–4(c) summarize the carrier densities and respective mobilities for the three films measured at various temperatures. The carrier densities and mobilities for the M phase as well as for its high temperature metallic R phase are comparable to the literature values.[20] VO_2(B) film shows a ~6 orders of decrease in carrier density from 5×10^{22} cm^{-3} (comparable to that of metallic R phase) to 1×10^{17} cm^{-3} accompanied by an increase of 2 orders of magnitude in mobility from 0.03 to 2.15 cm^2 V^{-1} s^{-1} measured at 300 K and

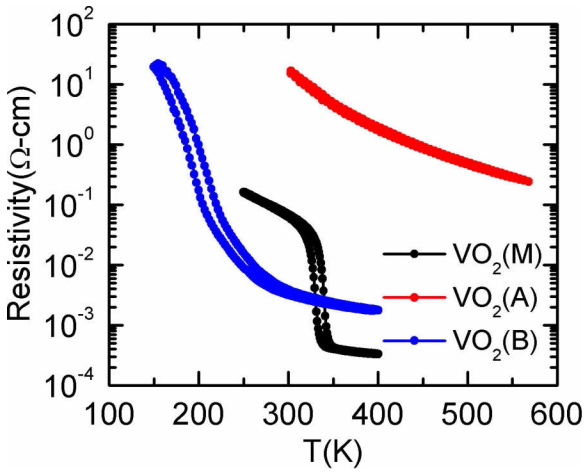

FIG. 3. Temperature dependent resistivity for VO_2(M), VO_2(A), and VO_2(B) films deposited on $SrTiO_3$ substrate.

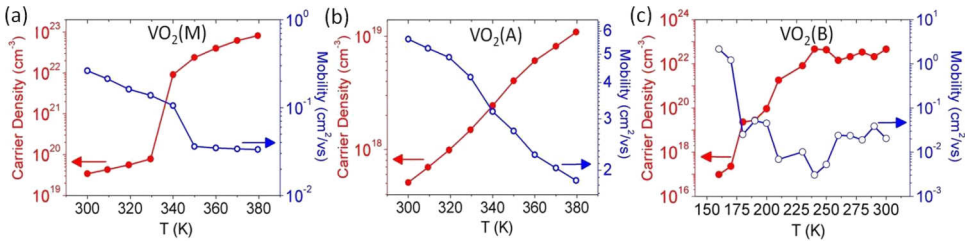

FIG. 4. (a), (b), and (c) Temperature dependent carrier density and mobility for VO_2(M), VO_2(A), and VO_2(B) films deposited on $SrTiO_3$ substrate.

150 K, respectively. Room temperature carrier density of VO_2(A) (1×10^{17} cm^{-3}) is comparable to that of VO_2(B) at low temperature (150 K) which is 2 orders of magnitude less than the VO_2(M). The lower mobility for increased carrier density in VO_2 polymorphs indicates the role of carrier-carrier scattering in the electronic transport. No evidence of insulator to metal transition in VO_2(A) films at 162.8 °C was observed and this is not surprising as even in the bulk material, the observed transition was quite weak.[13] On the contrary, the transport measurement of VO_2(B) films supports the previous low-temperature X-ray studies on VO_2(B) which revealed an evolution from a high temperature monoclinic metallic phase to another monoclinic insulating phase at low temperature.[14]

Fig. 5 shows the valence band photo emission spectra of A, B, and M phases of VO_2 measured by hard X-ray photoelectron spectroscopy (HAXPES). The excitation energy and the Fermi level of VO_2 is calibrated using Au Fermi level spectra. Before measuring X-ray photo electron spectra of each of the samples, we have performed measurements on Au Fermi level and used this value of energy to calibrate the excitation energy. In Fig. 5(a), the broad and higher intensity feature between 2 eV and 9 eV binding energies arises primarily from O 2p states whereas the relatively lower intensity peaks nearer to the Fermi energy (E_F) are mainly contributed by V 3d-like states. We focus on the V 3d related states in the vicinity of the E_F, shown in Fig. 5(b), that control the low energy excitations in these systems. Spectra for both VO_2(M) and VO_2(A) phases exhibit a single peak structure with no spectral intensity at the Fermi energy, consistent with the insulating state of both these compounds. These spectral features correspond to the lower Hubbard band of these strongly correlated systems and often have been termed the incoherent feature. The band gaps estimated from these spectra are

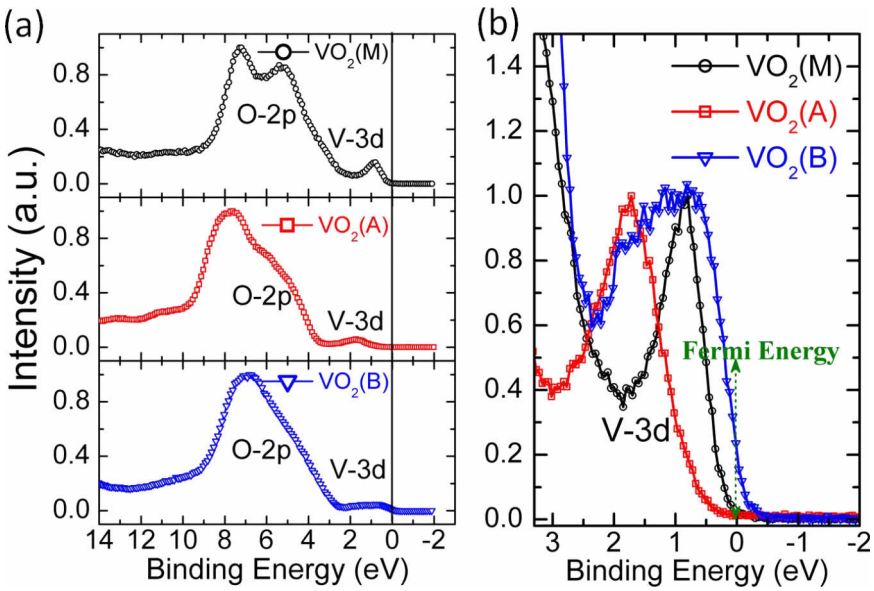

FIG. 5. (a) and (b) Bulk sensitive x-ray photoelectron spectroscopy (HAXPES) spectra taken at 300 K using photon energy 3.5 keV.

approximately 0.32 eV and 0.72 eV for the VO_2(M) and VO_2(A) phases, respectively. Band gaps are calculated based on the assumption that the conduction band is pinned close to the Fermi energy (i.e., the energy gap between the conduction band and the Fermi level is assumed to be very small.). In contrast, VO_2(B) phase V 3d spectral feature is relatively broad in nature. The broad spectral feature suggests two partially overlapping peaks in this case, with one peak position at about 1.6 eV, while the other at about 0.6 eV binding energy. The feature at the 1.6 eV binding energies appears between the spectral features of the lower Hubbard band in VO_2(M) and VO_2(A) phases, and can, therefore, be attributed to the incoherent spectral feature of the lower Hubbard band in VO_2(B) phase. The remaining feature, much closer to and with a finite intensity at the Fermi energy, clearly establishes the metallic nature of VO_2(B) phase at the room temperature; this low energy spectral feature is called the coherent peak in this case. Thus, the photoemission spectra for all three phases are consistent with the observed transport properties of VO_2 in these three phases.

In conclusion, we have shown that the three polymorphs of VO_2(A, B, and M) thin films can be prepared in single phase by controlling the vanadium arrival rate and the oxygen pressure both on $SrTiO_3$. The phase diagram for the growth of the various phases indicates that the VO_2(M/R) is the most stable phase, next is VO_2(A) followed by VO_2(B) as the least stable phase. The transport studies indicate that B is semi-metallic, A is insulating, while M is semiconducting which is corroborated by the HAXPES measurements. Thus, control of cationic and anionic atomic arrival rates is a powerful processing step for the growth of novel functional polymorphic materials.

We acknowledge the NUSNNI-NanoCore at the National University of Singapore, Singapore for the support. We would like to acknowledge for financial support from NRF-CRP "Tailoring Oxide Electronics by Atomic Control" Grant No. NRF2008NRFCRP002-024, NUS YIA, NUS cross-faculty grant, FRC, and BMBF. We would like to thank W. Drube, Indranil Sarkar, and Sumanta Mukherjee in carrying out high-energy photoemission spectroscopy at Petar-III synchrotron source made accessible through a program of the Nano-Mission, Department of Science and Technology, Government of India.

[1] M. Murdoch, G. I. N. Waterhouse, M. A. Nadeem, J. B. Metson, M. A. Keane, R. F. Howe, J. Llorca, and H. Idriss, Nat. Chem. **3**, 489 (2011).
[2] M. Guignard, C. Didier, J. Darriet, P. Bordet, E. Elkaïm, and C. Delmas, Nat. Mater. **12**, 74 (2013).
[3] Y.-Y. Hu, Z. Liu, K.-W. Nam, O. J. Borkiewicz, J. Cheng, X. Hua, M. T. Dunstan, X. Yu, K. M. Wiaderek, L.-S. Du, K. W. Chapman, P. J. Chupas, X.-Q. Yang, and C. P. Grey, Nat. Mater. **12**, 1130 (2013).
[4] T. Anderson, F. Ren, S. Pearton, B. S. Kang, H.-T. Wang, C.-Y. Chang, and J. Lin, Sensors **9**, 4669 (2009).
[5] T.-Z. Shen, S.-H. Hong, and J.-K. Song, Nat. Mater. **13**, 394 (2014).
[6] J. Zhou, Y. Gao, Z. Zhang, H. Luo, C. Cao, Z. Chen, L. Dai, and X. Liu, Sci. Rep. **3**, 3029 (2013).
[7] H. Katzke, P. Tolédano, and W. Depmeier, Phys. Rev. B **68**, 024109 (2003).
[8] Y. F. Zhang, X. Z. Zhang, Y. Huang, C. Huang, F. Niu, C. G. Meng, and X. Y. Tan, Solid State Commun. **180**, 24 (2014).
[9] J. F. Liu, Q. H. Li, T. H. Wang, D. P. Yu, and Y. D. Li, Angew. Chem., Int. Ed. **43**, 5048 (2004).
[10] H. Miyazaki and I. Yasui, Appl. Surf. Sci. **252**, 8367 (2006).
[11] Y. Muraoka and Z. Hiroi, Appl. Phys. Lett. **80**, 583 (2002).
[12] C. Marini, E. Arcangeletti, D. D. Castro, L. Baldassare, A. Perucchi, S. Lupi, L. Malavasi, L. Boeri, E. Pomjakushina, K. Conder, and P. Postorino, Phys. Rev. B **77**, 235111 (2008).
[13] Y. Oka, T. Ohtani, N. Yamamoto, and T. Takada, J. Ceram. Soc. Jpn. **97**, 1134 (1989).
[14] Y. Oka, T. Yao, N. Yamamoto, Y. Ueda, and A. Hayashi, J. Solid State Chem. **105**, 271 (1993).
[15] A. Chen, Z. Bi, W. Zhang, J. Jian, Q. Jia, and H. Wang, Appl. Phys. Lett. **104**, 071909 (2014).
[16] J. Hou, J. Zhang, Z. Wang, Z. Zhang, and Z. Ding, RSC Adv. **4**, 18055 (2014).
[17] See supplementary material at http://dx.doi.org/10.1063/1.4906880 for X-Ray reciprocal space map and rocking curve using 2D detector for VO_2 thin films M, A, and B (Figs. S1 and S2, Table S1); stoichiometry of VO_2(A) and VO_2(B) thin films using oxygen resonance Rutherford backscattering spectra (Fig. S3); dlog(R)/dT versus temperature plot for VO_2 polymorphs (Fig. S4).
[18] C. Leroux, G. Nihoul, and G. V. Tendeloo, Phys. Rev. B **57**, 5111 (1998).
[19] S. R. Popuri, A. Artemenko, C. Labrugere, M. Miclau, A. Villesuzanne, and M. Pollet, J. Solid State Chem. **213**, 79 (2014).
[20] M. Nakano, K. Shibuya, D. Okuyama, T. Hatano, S. Ono, M. Kawasaki, Y. Iwasa, and Y. Tokura, Nature **487**, 459 (2012).
[21] D. Ruzmetov, D. Heiman, B. B. Claflin, V. Narayanamurti, and S. Ramanathan, Phys. Rev. B **79**, 153107 (2009).
[22] S. A. Corr, M. Grossman, Y. Shi, K. R. Heier, G. D. Stucky, and R. Seshadri, J. Mater. Chem. **19**, 4362 (2009).